RSC Advances

PAPER

View Article Online
View Journal | View Issue

Cite this: *RSC Adv.*, 2025, **15**, 4952

Carbon dot-based fluorescent sensor for selective and sensitive detection of persulfate†

Tingyu Zhang, *[ab] Tingting Cai,[a] Yi Zhang[a] and Tanlai Yu [ab]

Received 20th December 2024
Accepted 6th February 2025

DOI: 10.1039/d4ra08915d

rsc.li/rsc-advances

Persulfate, a powerful oxidizing agent, is extensively employed in numerous industries. Accurate and rapid detection of persulfate ($S_2O_8^{2-}$) is essential. This study reports the development of a fluorescent sensor based on Am-CDs. It is synthesized from ascorbic acid (AA) and *m*-phenylenediamine (m-PD) through a one-step hydrothermal method. The fluorescence of Am-CDs demonstrated selective sensitivity to $S_2O_8^{2-}$ *via* static quenching. A sensitive fluorescent sensor was constructed for $S_2O_8^{2-}$, exhibiting a linear detection range of 1.96 to 15.59 μM with a limit of detection (LOD) of 0.94 μM. This fluorescence method was successfully applied to detect $S_2O_8^{2-}$ in water samples, achieving recoveries of 98.07% to 102.33%. The fluorescent sensor developed in this study offers a simple and effective method for quantifying $S_2O_8^{2-}$ in aquatic environments.

1 Introduction

Persulfate is an effective oxidizing agent extensively used in industries such as water and soil detergents,[1] circuit board manufacturing,[2] cosmetics,[3] and polymerization processes.[4] Evidence suggests that exposure to persulfate may exacerbate conditions like asthma,[5] underscoring the need for its detection. Conventional methods for persulfate determination include iodometric titration, reduction techniques, polarographic spectrophotometry, chemiluminescence, and ion chromatography.[6] However, these approaches present challenges, such as procedural complexity and slower response times, which restrict broader application. Fluorescence sensing methods offer notable advantages, including high sensitivity, good selectivity, and operational simplicity, making the development of fluorescence-based detection strategies for persulfates essential.

Carbon dots (CDs) are zero-dimensional carbon-based nanomaterials recognized for their light-emitting properties. These materials offer numerous advantages, including superior optical stability,[7] biocompatibility,[8] low toxicity,[9] and ease of synthesis.[10] As a result, CDs are employed in diverse applications such as catalysis,[11] printing inks,[12] biological imaging,[13,14] and electronic devices.[15] Due to their remarkable attributes, CDs have gained prominence as fluorescent probes for detecting and analyzing various targets.[16] Increasing research highlights the utility of CDs in detecting metal ions,[17] anions,[18] and organic compounds[19] across environments, including biomedical and food systems. However, limited studies focus on the detection of persulfate anions using CDs. For instance, a nanocomposite comprising dual emission CQDs-Zn^{2+} was designed to detect $S_2O_8^{2-}$ but exhibited low sensitivity and required a non-pure water system, limiting practical applications.[20] Similarly, a four-channel detection platform for $S_2O_8^{2-}$ was developed; however, its purification process proved complex and time-intensive.[21]

In this study, carbon dots (Am-CDs) were synthesized from ascorbic acid (AA) and *m*-phenylenediamine (m-PD) *via* a simple one-step hydrothermal process. The designation 'Am-CDs' was derived from the precursor's name as a prefix.[22] The prepared Am-CDs did not require complex purification methods and could be obtained through a simple two-step filtration, thereby reducing the material preparation time. Furthermore, there was no need to dope with metal elements, avoiding potential environmental hazards. The resulting Am-CDs exhibit excellent water solubility, photostability, and fluorescence properties. Notably, the fluorescence of Am-CDs is efficiently quenched by $S_2O_8^{2-}$ through a static quenching mechanism. On the basis of this property, a fluorescence probe for $S_2O_8^{2-}$ detection was developed and successfully applied to analyze $S_2O_8^{2-}$ in real-world samples. The development of this fluorescence probe based on Am-CDs represents a novel approach within the field of detection methods, which are critical for effective monitoring and analysis.

2 Experimental

2.1 Materials

Ascorbic acid and *m*-phenylenediamine were procured from Aladdin Reagents Company (Shanghai, China). All reagents

[a]*Department of Chemistry and Material Engineering, Lyuliang University, Lyuliang 033000, P. R. China*

[b]*Institute of New Carbon-based Materials and Zero-carbon and Negative-carbon Technology,Lyuliang University, Lyuliang 033000, P. R. China. E-mail: zty@llu.edu.cn*

† Electronic supplementary information (ESI) available. See DOI: https://doi.org/10.1039/d4ra08915d

used were of analytical grade. The water utilized in the experiments was ultrapure deionized water. No further purification was performed on any of the chemicals.

2.2 Preparation of Am-CDs

Am-CDs were prepared using a one-step hydrothermal method. Specifically, 0.20 g of ascorbic acid and 0.30 g of *m*-phenylenediamine were dissolved in 10 mL of ultrapure water, followed by ultrasonic dispersion for 20 min. The mixture was transferred into a 50 mL Teflon-lined autoclave and heated at 200 °C for 8 h. Upon cooling to room temperature, the product was initially filtered using filter paper to remove large particles and then passed through a 0.22 μm microporous membrane for further purification. The resulting solution was lyophilized to yield solid Am-CDs, which were stored at 4 °C for subsequent experimental use.

2.3 Measurement of fluorescence quantum yield

The fluorescence quantum yield (QY) of Am-CDs was determined using the following formula:

$$\Phi_S = \Phi_R(\mathrm{Grad}_S/\mathrm{Grad}_R)\cdot(\eta_S^2/\eta_R^2)$$

where Grad and η represent the slope of absorbance *versus* the integrated fluorescence spectrum area and the refractive index, respectively. The subscripts "S" and "R" denote the sample and the standard, respectively. Quinine sulfate dissolved in 0.1 M H_2SO_4 was used as the standard with a QY of 0.54.

2.4 Detection of $S_2O_8^{2-}$

The detection of $S_2O_8^{2-}$ was carried out at room temperature. For a typical measurement, a homogeneous solution was prepared by adding 2 mL of Am-CDs aqueous solution (10 mg mL^{-1}) into a fluorescence cuvette. Fluorescence titration was conducted to determine the linear range and detection limit for $S_2O_8^{2-}$. All measurements were performed at an excitation wavelength (λ_{ex}) of 410 nm.

2.5 Detection of $S_2O_8^{2-}$ in actual samples

Water samples were collected from tap water and Daming Lake water in Lyvliang University. These samples were filtered using

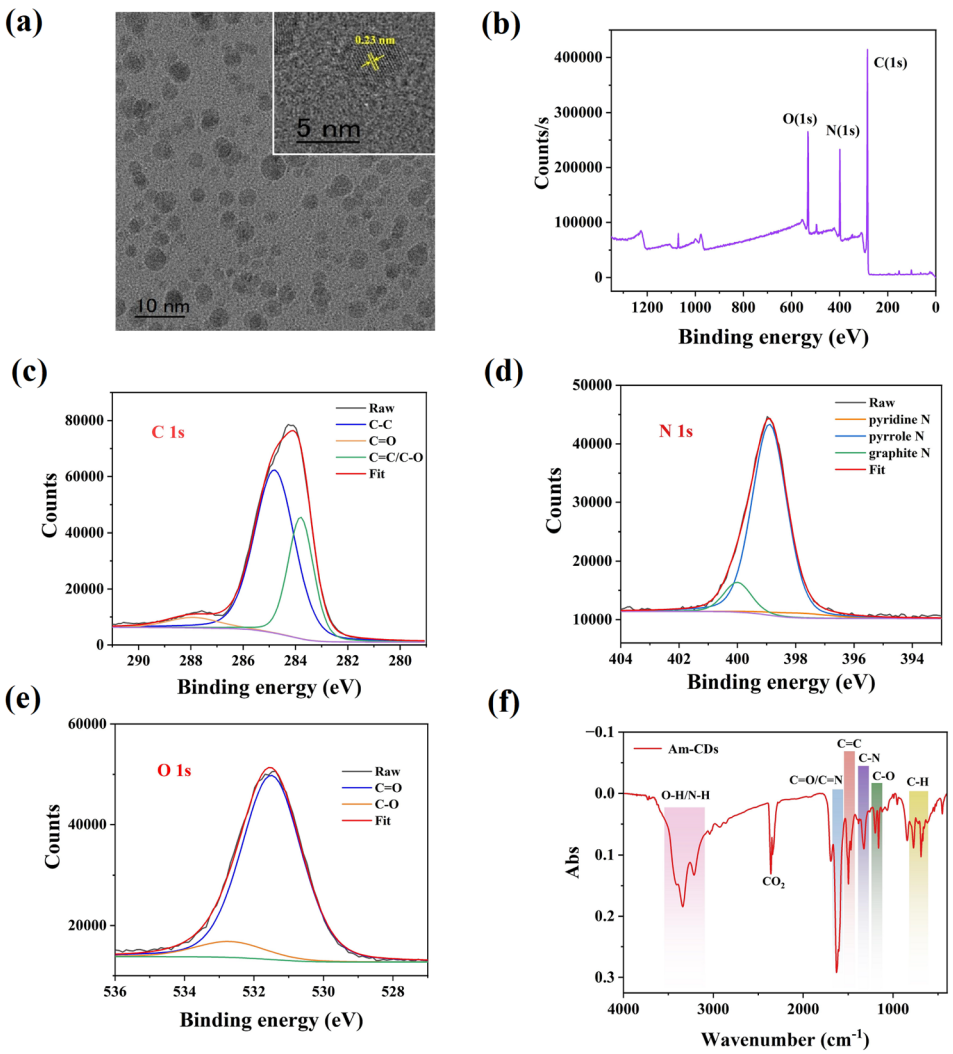

Fig. 1 (a) TEM image of Am-CDs. (b) Full survey XPS spectra. High-resolution spectra of (c) C 1s, (d) N 1s, and (e) O 1s. (f) FTIR spectra of Am-CDs.

a 0.22 μm microporous membrane. The concentration of $S_2O_8^{2-}$ in these water samples was determined, and the recovery rate of spiked samples was calculated.

3 Results and discussion

3.1 Characterization of the Am-CDs

The morphology and size of Am-CDs were characterized using transmission electron microscopy (TEM). The TEM image in Fig. 1a demonstrates that the Am-CDs were spherical with notable dispersity and a lattice spacing of about 0.23 nm. The average particle size was determined to be 7.69 ± 0.41 nm (Fig. S1†). To identify the functional groups present on the surfaces of Am-CDs, X-ray photoelectron spectroscopy (XPS) and Fourier-transform infrared (FTIR) spectroscopy were utilized. The full XPS spectrum (Fig. 1b) revealed three distinct bands at 531.53, 398.92, and 284.25 eV, corresponding to O 1s, N 1s, and C 1s, respectively. Deconvolution of the C 1s spectrum identified three peaks at 284.8, 286.1, and 288.2 eV, attributed to C=C/C–O, C–C, and C=O groups, respectively (Fig. 1c). In the N 1s spectrum, three peaks at 398.2, 399.2, and 400.3 eV indicated the presence of pyridine N, pyrrolic N, and graphitic N, with pyrrolic N being the predominant form (Fig. 2d). The O 1s spectrum displayed two peaks at 531.5 and 532.7 eV, corresponding to C=O and C–O, respectively (Fig. 1e). The FTIR spectrum of Am-CDs showed a broad peak around 3340 cm^{-1}, indicative of hydroxyl (–OH) groups on the surface. A double peak near 2350 cm^{-1} (2341 and 2360 cm^{-1}) was assigned to CO_2 gas absorbed from the air.[23] Additional absorption peaks at 1629, 1497, 1325, 1198, and 772 cm^{-1} were associated with the stretching vibrations of C=O/C=N, C=C, C–N, C–O, and C–H groups, respectively.[24,25] These observations confirm that the synthesis of Am-CDs led to the incorporation of numerous hydrophilic and oxygenated reactive functional groups.

3.2 Optical properties of the Am-CDs

The ultraviolet-visible (UV-vis) absorption spectrum of the aqueous Am-CDs solution (purple line) exhibited a distinct peak at 223 nm, corresponding to the π–π* and n–π* transitions of C=C and sub-fluorescent groups, respectively (Fig. 2a).[26] A weak absorption peak observed at 288 nm was attributed to the n–π* transition of C=O/C=N groups.[27] The optimal excitation and emission wavelengths (green and red lines) were identified at 410 and 514 nm, respectively, with a Stokes shift of 96 nm. The three-dimensional (3D) fluorescence spectra of Am-CDs under varying excitation wavelengths (Fig. 2b) revealed a slight red shift of the emission peak as the excitation wavelength increased from 310 nm to 460 nm. This excitation-dependent emission behavior, commonly observed in carbon dots, is associated with the π* → n transition of surface-attached functional groups.[28]

The stability of Am-CDs was assessed to determine their suitability for practical applications (Fig. 2c). The fluorescence intensity of Am-CDs showed negligible variation across NaCl concentrations ranging from 0.5 to 3.0 M and H_2O_2 concentrations between 0.1 and 1.0 M. However, fluorescence intensity decreased significantly in strong acidic and alkaline conditions. The addition of acid leads to the protonation of CDs surface functional groups, such as amino groups, generating luminescent quencher sites and resulting in a decrease in emission intensity.[29] When the pH exceeded 10, a significant reduction in fluorescence intensity was observed. This change is primarily attributed to the varying ionization degrees of the functional groups within the CDs framework as a result of pH variation, which directly affects the deprotonation levels and

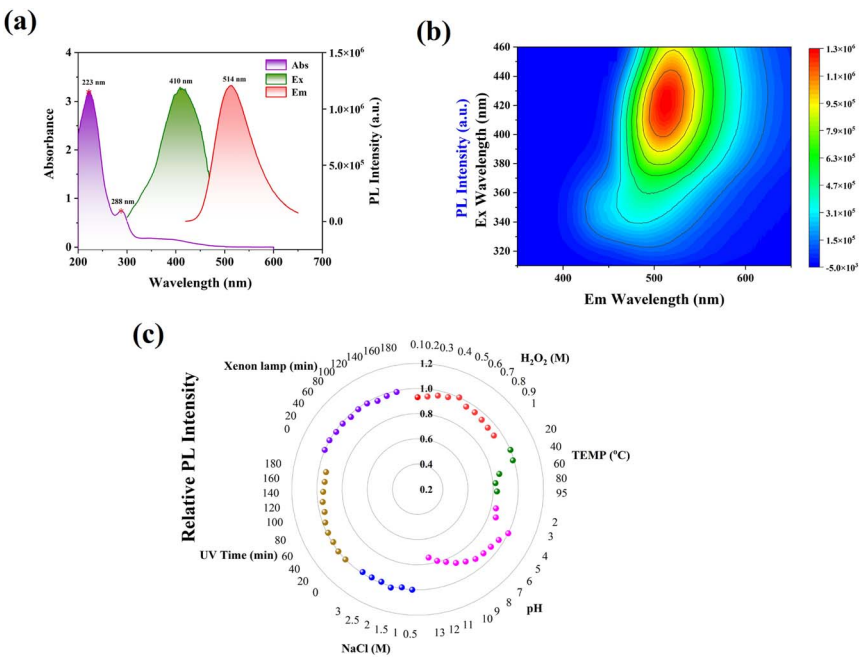

Fig. 2 (a) UV absorption, excitation, and emission spectra of Am-CDs. (b) 3D fluorescence emission spectra. (c) Stability of Am-CDs.

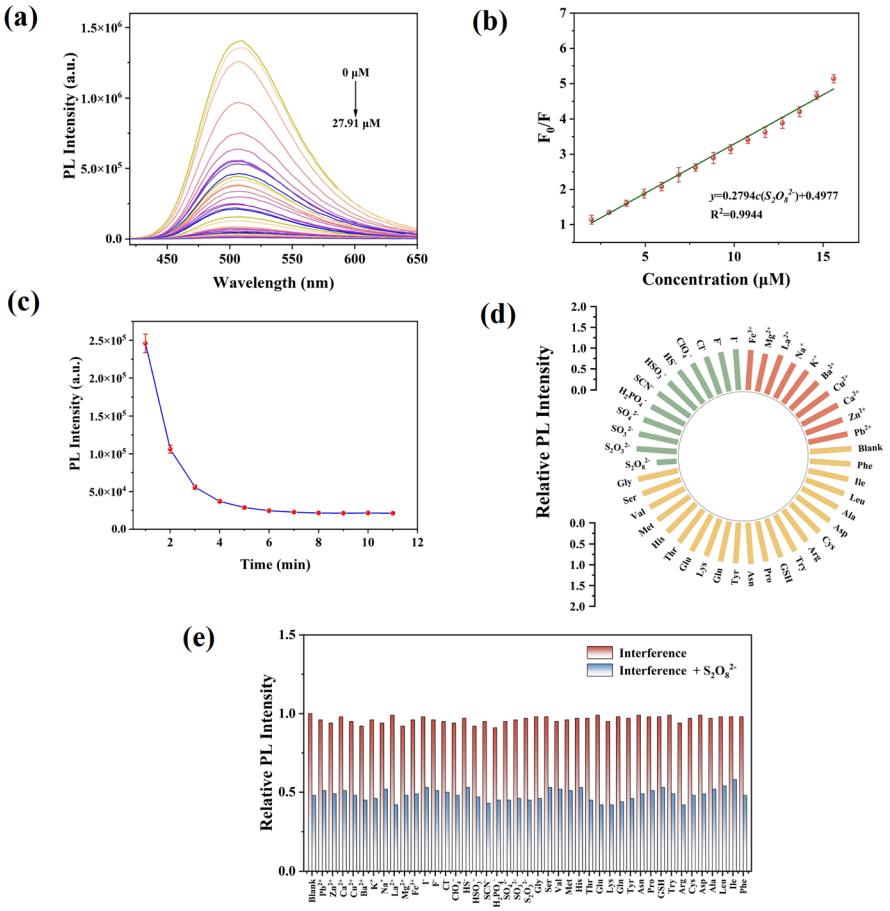

Fig. 3 (a) Fluorescence quenching of Am-CDs in the presence of $S_2O_8^{2-}$ (0–27.91 μM). (b) Linear relationship between F_0/F and $S_2O_8^{2-}$ concentration (1.96–15.59 μM). (c) Reaction time of the system. (d and e) Selectivity and anti-interference patterns of the system, respectively.

consequently alters the fluorescence properties.[30] A pronounced reduction in fluorescence was also observed when the temperature exceeded 40 °C. This phenomenon can be attributed to the thermally activated population of non-radiative channels associated with surface trap or defect states.[31,32] As the temperature increases, a greater number of non-radiative channels become activated, resulting in more excited electrons transitioning back to the ground state *via* non-radiative processes.[33] Consequently, the fluorescence intensity decreases. This result limits its application in high-temperature environments. Notably, the fluorescence intensity remained stable after 180 minutes of continuous exposure to UV light and xenon lamp irradiation. The QY of Am-CDs, calculated using quinine sulfate as a reference, was determined to be 18.4%.

3.3 Detection of $S_2O_8^{2-}$

As depicted in Fig. 3a, the fluorescence intensity of the Am-CDs aqueous solution reduced as the concentration of $S_2O_8^{2-}$ increased from 0 to 27.91 μM. The titration curve of Am-CDs with varying concentrations of $S_2O_8^{2-}$ is presented in the Fig. S2.† At higher concentrations, a significant increase in the F_0/F ratio was observed. This phenomenon may be attributed to the formation of more non-fluorescent ground state complexes, which suppress the fluorescence of the remaining carbon dots. A strong linear correlation was observed between 1.96–15.59 μM (Fig. 3b). The linear equation is $F_0/F = 0.2794c(S_2O_8^{2-}) + 0.4977$ ($R^2 = 0.9944$). The LOD was calculated to be 0.94 μM, which was based on three times the standard deviation rule.

$$\mathrm{LOD} = 3\sigma/S$$

Table 1 Comparison of detection methods

Material	Method	Linger range (μM)	LOD (μM)	Ref.
RF/GQDs/GC	Electrochemistry	1–1000	0.2	34
DCSB-MoNCs	Fluorescence	25–55	3.43	35
NBIM	Fluorescence	0–7	0.0052	36
CQDs	Fluorescence	20–300	8.3	21
Am-CDs	Fluorescence	1.96–15.59	0.94	This work

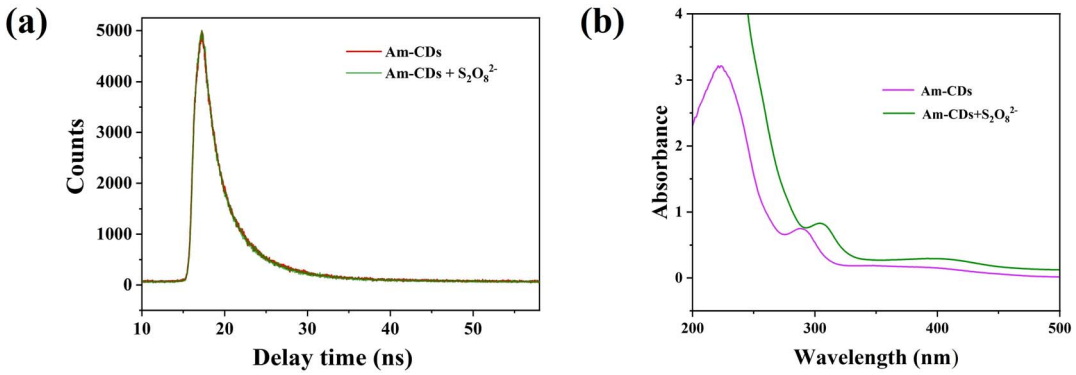

Fig. 4 (a) Fluorescence decay curve of Am-CDs without and with $S_2O_8^{2-}$. (b) UV-vis absorption spectra of Am-CDs without and with $S_2O_8^{2-}$.

Here, σ represents the standard deviation of six blank measurements, and S represents the slope of the calibration curve. The system showed a reaction time of 6 min (Fig. 3c).

Selectivity and anti-interference capabilities are essential for effective detection systems. The selectivity of the Am-CDs system was evaluated using various metal ions (orange bars), anions (green bars), and amino acids (yellow bars) (Fig. 3d). Except for $S_2O_8^{2-}$, none of the tested interfering substances caused quenching of the fluorescence intensity, indicating strong specificity for $S_2O_8^{2}$ detection. In our comparison, we utilized m-PD as the sole carbon source to synthesize carbon dots under identical conditions, which exhibited no response to $S_2O_8^{2-}$. This finding suggests that AA is crucial for the detection of $S_2O_8^{2-}$. The AA molecules possess their own conjugated double bonds and have a low molecular weight, which may influence the selectivity of the Am-CDs. Furthermore, the Am-CDs system exhibited robust anti-interference performance in the presence of other substances, as shown in Fig. 3e.

Compared with the reported methods (Table 1), the linear range for Am-CDs was 1.96–15.59 μM, which was narrower than that of RF/GQDs/GC (1–1000 μM) and CQDs (20–300 μM). This indicated that Am-CDs exhibit higher sensitivity and selectivity within a specific concentration range. The LOD was lower than that of most materials listed in the table, although it was not as favorable as the electrochemistry method. However, compared with the fluorescence detection of carbon dots, the performance was notably excellent. This finding is significant for exploring the potential applications of carbon dots.

3.4 Quenching mechanism

To investigate the mechanism for the detection of $S_2O_8^{2-}$, the fluorescence lifetime was measured. As shown in Fig. 4a, the average fluorescence lifetime of the Am-CDs was found to be 3.24 ns. Upon the addition of $S_2O_8^{2-}$, the average lifetime increased to 3.31 ns. The fluorescence lifetime of Am-CDs remained almost constant with the addition of $S_2O_8^{2}$, suggesting the occurrence of a static quenching process. Static quenching occurs when a non-fluorescent ground-state complex is formed through the interaction between the CDs and the quencher. The complex immediately returns to the ground state without emission of a photon when the complex absorbs light.[37] The formation of the ground-state complex can change the absorption spectrum of the CDs. A notable change in the UV-vis absorption of Am-CDs was observed after the addition of $S_2O_8^{2-}$ (Fig. 4b). The absorption peak at 223 nm disappeared, whereas a new absorption peak emerged at 400 nm, further indicating the formation of non-fluorescent ground state complexes. As shown in Fig. S3,† the UV-vis absorption spectrum of $S_2O_8^{2-}$ did not overlap with the fluorescence excitation and emission spectra of Am-CDs, which further supports the static quenching mechanism.

Table 2 Analytical results for the detection of $S_2O_8^{2-}$ in real samples

Sample	Add (μM)	Detected (μM)	RSD (%, $n = 6$)	Recovery (%)
Tap water	5	5.12	2.36	102.33
	10	9.81	3.74	98.07
Lake water	5	5.08	3.87	101.67
	10	10.08	2.98	100.77

3.5 Application in actual samples

Water samples from both a tap and Daming Lake were collected and analyzed. As presented in Table 2, the sample recoveries varied from 98.07% to 102.33%, with relative standard deviations (RSDs) ranging from 2.36% to 3.87% ($n = 6$) for the water samples. These findings suggest that the Am-CDs-based sensor can reliably and efficiently measure the$S_2O_8^{2-}$ concentration in real samples.

4 Conclusion

In conclusion, a sensor for the selective and accurate determination of $S_2O_8^{2-}$ content in water samples was successfully developed using Am-CDs. The Am-CDs were synthesized through a simple one-step hydrothermal process involving ascorbic acid (AA) and *m*-phenylenediamine (m-PD). The fluorescence of the Am-CDs was effectively quenched by $S_2O_8^{2-}$, attributed to the mechanism of static quenching. Additionally, the applicability of the constructed sensor was demonstrated by determining $S_2O_8^{2-}$ content in water samples.

Data availability

The authors conform that the data supporting the findings are available within the main article.

Author contributions

All authors contributed to the study conception and design. T. Y. Zhang: conceptualization, data curation, formal analysis, investigation, methodology, and writing – original draft; T. T Cai: review and editing; Y. Zhang: methodology, conceptualization, formal analysis; T. L. Yu: investigation and methodology. All authors read and approved the final manuscript.

Conflicts of interest

There is no conflict to declare.

Acknowledgements

This work was supported by The Science and Technology Plan Project of Lyuliang (No. 2023GXYF06), Fundamental Research Program of Shanxi Province (No. 202303021212284) and Teaching Reform and Innovation Programs of Higher Education Institutions in Shanxi (J20231331).

References

1 P. F. Killian, C. J. Bruell, C. Liang and M. C. Marley, *Soil Sediment Contam.: Int. J.*, 2007, **16**, 523–537.
2 J. Branson, J. Naber and G. Edelen, *IEEE Trans. Educ.*, 2000, **43**, 257–261.
3 T. Mensing, W. Marek, M. Raulf-Heimsoth and X. Baur, *Eur. Respir. J.*, 1998, **12**, 1371–1374.
4 H. Lin, *Eur. Polym. J.*, 2001, **37**, 1507–1510.
5 X. Muñoz, M.-J. Cruz, R. Orriols, C. Bravo, M. Espuga and F. Morell, *Chest*, 2003, **123**, 2124–2129.
6 N. E. Khan and Y. G. Adewuyi, *J. Chromatogr. A*, 2011, **1218**, 392–397.
7 Z. Savari, S. Soltanian, A. Noorbakhsh, A. Salimi, M. Najafi and P. Servati, *Sens. Actuators, B*, 2013, **176**, 335–343.
8 X. Wei, L. Li, J. Liu, L. Yu, H. Li, F. Cheng, X. Yi, J. He and B. Li, *ACS Appl. Mater. Interfaces*, 2019, **11**, 9832–9840.
9 P. Yang, Z. Zhu, T. Zhang, W. Zhang, W. Chen, Y. Cao, M. Chen and X. Zhou, *Small*, 2019, **15**, 1902823.
10 W. Li, S. Wu, X. Xu, J. Zhuang, H. Zhang, X. Zhang, C. Hu, B. Lei, C. F. Kaminski and Y. Liu, *Chem. Mater.*, 2019, **31**, 9887–9894.
11 S. Cailotto, R. Mazzaro, F. Enrichi, A. Vomiero, M. Selva, E. Cattaruzza, D. Cristofori, E. Amadio and A. Perosa, *ACS Appl. Mater. Interfaces*, 2018, **10**, 40560–40567.
12 J. Xu, K. Cui, T. Gong, J. Zhang, Z. Zhai, L. Hou, F. U. Zaman and C. Yuan, *Nanomaterials*, 2022, **12**, 312.
13 M. Tian, J. Zhang, Y. Liu, Y. Wang and Y. Zhang, *Spectrochim. Acta, Part A*, 2021, **252**, 119541.
14 L. Li, L. Shi, J. Jia, Y. Jiao, Y. Gao, Y. Liu, C. Dong and S. Shuang, *Spectrochim. Acta, Part A*, 2020, **227**, 117716.
15 T. Feng, S. Tao, D. Yue, Q. Zeng, W. Chen and B. Yang, *Small*, 2020, **16**, 2001295.
16 S. Liao, X. Huang, H. Yang and X. Chen, *Anal. Bioanal. Chem.*, 2018, **410**, 7701–7710.
17 S. Mohandoss, S. Ganesan, S. Palanisamy, S. You, K. Velsankar, S. Sudhahar, H.-M. Lo and Y. R. Lee, *Chemosphere*, 2023, **313**, 137444.
18 L. Yan, B. Zhang, Z. Zong, W. Zhou, S. Shuang and L. Shi, *J. Colloid Interface Sci.*, 2023, **651**, 59–67.
19 D. Wang, X. Ding, J. Xie, J. Wang, G. Li and X. Zhou, *Anal. Chim. Acta*, 2024, **1285**, 342025.
20 D. Bu, H. Song, Z. Li, L. Wei, H. Zhang and M. Yu, *Luminescence*, 2020, **35**, 1319–1327.
21 D. Xu, H. Xu, Q. Long, J. Yu, Y. Wang and P. Zhang, *Mater. Lett.*, 2022, **318**, 132183.
22 Q. Zeng, T. Feng, S. Tao, S. Zhu and B. Yang, *Light:Sci. Appl.*, 2021, **10**, 142.
23 T. Yoshinaga, Y. Iso and T. Isobe, *ECS J. Solid State Sci. Technol.*, 2018, **7**, R3034–R3039.
24 Y. Han, X. Kong, R. Bao, L. Yi, Y. Gu, L. Liu, L. Lan, Z. Gan, J. Yi and X. Zhang, *ACS Appl. Nano Mater.*, 2024, **7**, 1674–1683.
25 H. S. Al-mashriqi, P. Sanga, J. Chen, E. Qaed, J. Xiao, X. Li and H. Qiu, *Carbon*, 2024, **228**, 119380.
26 Z. Yang, T. Xu, H. Li, M. She, J. Chen, Z. Wang, S. Zhang and J. Li, *Chem. Rev.*, 2023, **123**, 11047–11136.
27 M. Kr. Mahto, D. Samanta, M. Shaw, M. A. S. Shaik, R. Basu, I. Mondal, A. Bhattacharya and A. Pathak, *ACS Appl. Nano Mater.*, 2023, **6**, 8059–8070.
28 X. Gong, H. Wang, Y. Liu, Q. Hu, Y. Gao, Z. Yang, S. Shuang and C. Dong, *Anal. Chim. Acta*, 2019, S0003267019300510.
29 Z. Sun, W. Zhou, J. Luo, J. Fan, Z. Wu, H. Zhu, J. Huang and X. Zhang, *J. Colloid Interface Sci.*, 2022, **607**, 16–23.
30 G. Yang, X. Wan, Y. Su, X. Zeng and J. Tang, *J. Mater. Chem. A*, 2016, **4**, 12841–12849.
31 P. Yu, X. Wen, Y.-R. Toh and J. Tang, *J. Phys. Chem. C*, 2012, **116**, 25552–25557.
32 Z. Song, F. Quan, Y. Xu, M. Liu, L. Cui and J. Liu, *Carbon*, 2016, **104**, 169–178.
33 D. Chang, L. Shi, Y. Zhang, G. Zhang, C. Zhang, C. Dong and S. Shuang, *Analyst*, 2020, **145**, 2176–2183.
34 M. Roushani and Z. Abdi, *Sens. Actuators, B*, 2014, **201**, 503–510.
35 M. R. Kateshiya, D. J. Joshi, M. Anil Kumar, N. I. Malek and S. Kumar Kailasa, *J. Mol. Liq.*, 2022, **365**, 120139.
36 S. Zhang, M. Qiao, T. Liu, L. Ding and Y. Fang, *Sens. Actuators, B*, 2022, **365**, 131931.
37 F. Zu, F. Yan, Z. Bai, J. Xu, Y. Wang, Y. Huang and X. Zhou, *Microchim. Acta*, 2017, **184**, 1899–1914.